HHS Public Access
Author manuscript
*Magn Reson Med*. Author manuscript; available in PMC 2017 January 01.

Published in final edited form as:
*Magn Reson Med*. 2016 January ; 75(1): 345–355. doi:10.1002/mrm.25649.

# Assessment of lymphatic impairment and interstitial protein accumulation in patients with breast cancer treatment-related lymphedema using CEST MRI

**Manus J. Donahue**[1,4,*,^], **Paula C.M. Donahue**[5,6,^], **Swati Rane**[1], **Chris Thompson**[7], **Megan K. Strother**[1], **Allison Scott**[1], and **Seth A. Smith**[1]

[1] Department of Radiology, Vanderbilt School of Medicine, Nashville, TN

[2] Department of Psychiatry, Vanderbilt School of Medicine, Nashville, TN

[3] Department of Neurology, Vanderbilt School of Medicine, Nashville, TN

[4] Physics and Astronomy, Vanderbilt School of Medicine, Nashville, TN

[5] Physical Medicine and Rehabilitation, Vanderbilt School of Medicine, Nashville, TN

[6] Dayani Center for Health and Wellness, Nashville, TN

[7] Vanderbilt University Institute of Imaging Science, Vanderbilt School of Medicine, Nashville, TN

## Abstract

**Purpose—**Lymphatic impairment is known to reduce quality of life in some of the most crippling diseases of the 21st century, including obesity, lymphedema, and cancer. However, the lymphatics are not nearly as well-understood as other bodily systems, largely owing to a lack of sensitive imaging technologies that can be applied using standard clinical equipment. Here, proton exchange-weighted MRI is translated to the lymphatics in patients with breast cancer treatment-related lymphedema (BCRL).

**Methods—**Healthy volunteers (N=8) and BCRL patients (N=7) were scanned at 3T using customized structural MRI and amide proton transfer (APT) chemical exchange saturation transfer (CEST) MRI in sequence with the hypothesis that APT effects would be elevated in lymphedematous tissue. APT contrast, lymphedema stage, symptomatology, and histology information were evaluated.

**Results—**No significant difference between proton-weighted APT contrast in the right and left arms of healthy controls was observed. An increase in APT contrast in the affected arms of patients was found (P=0.025; Cohen's d=2.4), and variability among patients was consistent with documented damage to lymphatics as quantified by lymphedema stage.

---

[*] **Corresponding Author:** Manus J. Donahue, PhD, Vanderbilt Department of Radiology, Vanderbilt University Institute of Imaging Science, Medical Center North, 1161 21st Avenue South, Nashville, TN 37232, Tel: 615.322.8350, mj.donahue@vanderbilt.edu.

[^] Authors contributed equally to this work

**Prepared for**: Full Paper in *Magnetic Resonance in Medicine*

**Declaration of conflict of interest:** The authors declare that no conflict of interest exists

Author Manuscript
Author Manuscript
Author Manuscript
Author Manuscript

Author Manuscript

Author Manuscript

Author Manuscript

Author Manuscript

**Conclusions—**APT CEST MRI may have relevance for evaluating lymphatic impairment in patients with BCRL, and may extend to other pathologies where lymphatic compromise is evident.

**Keywords**

CEST; APT; lymphedema; breast cancer; lymphatic; MRI

## Introduction

The lymphatic system is one of the most poorly understood and oftentimes overlooked bodily systems, yet is fundamental to a spectrum of devastating diseases, including infection, cancer, cancer-treatment morbidity, cardiovascular disease, and obesity (1). The ability to grow technologies that can be applied readily in clinical settings to evaluate lymphatic structure and function is likely fundamental to improving our understanding of the lymphatic system, identifying patients with early failure of compromised lymphatics, and ultimately titrating therapies that may prevent or delay complication onset.

The lymphatic system is part of the circulatory system and consists of a network of lymphatic vessels and nodes whose purpose is to maintain fluid balance, as well as to process and return capillary ultrafiltrate and plasma proteins back to the blood circulation. In most tissues, lymphatic capillaries remove arterial capillary fluid efflux that would otherwise accumulate in the interstitium (extracellular tissue). Once the fluid enters the lymphatic capillaries, it is referred to as lymphatic fluid and the fluid volume is referred to as the lymphatic load. The capillary ultrafiltrate is drained by lymphatic vessels, processed by lymphatic nodes, and returned to the blood circulation. When the lymphatic transport capacity (i.e., highest possible lymphatic flow per unit time) exceeds the lymphatic load, fluid balance is disrupted, protein-rich fluid accumulates in the interstitium, and macroscopic swelling, or lymphedema, results (2).

Lymphedema is one of the most frequent complications of breast cancer treatment, which often includes radiation and/or surgical resection of lymph nodes, and breast cancer treatment-related lymphedema (BCRL) specifically has a mean incidence of approximately 30% (3). In patients with such secondary lymphedema, an inability of remaining lymphatic vessels and nodes not damaged by treatment to adequately process the lymphatic load, known as mechanical insufficiency, results in an accumulation of protein rich fluid in the dependent tissues leading to swelling of the involved arm and/or upper truncal quadrant (4-6).

Despite the high prevalence of BCRL and associated physical and quality of life issues for patients, there is no cure and therapeutic trials are limited. Identification of patients at increased risk for BCRL is currently not possible, yet identification of such patients could be used for titrating therapy regimes that could delay or reduce lymphedema severity. However, significant gaps in our knowledge remain regarding (i) how lymphatic functioning following cancer therapies, premorbid conditions (e.g., lymphatic structure, age and weight), and behavior modifications influence the development of BCRL and (ii) how emerging therapies impact lymphatic function and more specifically in which patients such therapies are required.

Author Manuscript Author Manuscript Author Manuscript Author Manuscript

Detection of early impairment and risk status followed by appropriate treatment intervention is likely crucial to reducing BCRL-related morbidity, as suggested in a recent study demonstrating that only 7% of patients receiving structured physical therapy (PT) develop BCRL in the first year, relative to 25% of PT-negative controls (7). However in practice, lymphedema prevention education and PT is inconsistently prescribed for patients owing to uncertainties regarding impact on prognosis and actual risk of BCRL. The fundamental barrier to understanding therapeutic efficacy and optimized treatment plans is that sensitive measures of lymphatic impairment, and thus objective trial end-points, remain underdeveloped. As such, clinical or research trials evaluating therapy impact on BCRL involve external limb measurements and extracellular fluid measurements (e.g., bioimpedance), which are helpful for quantifying general changes to fluid volume in the limb. However, these measurements are not designed to provide information on specific changes regarding lymphatic functioning of the arm and are unable to provide information about the involved upper truncal quadrant or bilateral arm involvement.

Interestingly, given the burden that lymphedema places on cancer survivors and health care systems (8,9), as well as the routine use of MRI for diagnostics, MRI techniques for assessing lymphatic structure and function are extremely limited (10-12). In BCRL, when cancer therapies disrupt the lymphatic system causing the lymphatic load to exceed the lymphatic transport capacity, protein accumulates in the interstitial space which left untreated will lead to protein-rich edema. It has not been possible to measure this protein accumulation using noninvasive imaging to date. MRI signal is almost always derived from protons on water molecules, however it is also possible to indirectly image labile protons associated with protein/peptide backbone constituents in very small concentrations using principles of chemical exchange. One of the most popular methods for sensitizing an MRI acquisition to labile protons is through chemical exchange saturation transfer (CEST), and specifically for amide protons resident on proteins and peptides, amide proton transfer (APT) imaging (13,14). Large field-of-view CEST APT MRI can be performed using standard equipment available at most hospitals and using commonplace imaging readouts optimized for structural and functional MRI. Chemical exchange information is obtained through saturation transfer of magnetization between amide protons (primarily on the peptide backbone; *in vivo* concentration = 70-100 mM) and the imaged water protons (concentration = 110 M). In CEST APT MRI, the contrast originates from amide (NH) protons resonating at 8.3 ppm in the proton spectrum (+3.5 ppm from water) (15). Over a physiological range of temperature constant pH, the exchange rate is primarily driven by the NH concentration. As NH groups are prominent on the peptide backbone, CEST APT contrast increases for increasing peptide concentration as has been demonstrated in a large amount of *ex vivo* and *in vivo* data (11,16,17).

Here, we apply APT CEST MRI for the first time in patients with BCRL with the overall hypothesis that elevated interstitial protein accumulation will lead to an enhancement of the APT effect in a manner that depends spatially on limb involvement and extent of lymphedema severity, and this contrast may be detectible even before clinical signs of swelling exist. The long-term goal of this work is to demonstrate abilities to accurately record structural and functional observables of lymphatic dysfunction, derived from

Author Manuscript Author Manuscript Author Manuscript Author Manuscript

noninvasive MRI equipment available at most hospitals, which can serve as trial end points for future rigorous, randomized clinical trials of lymphedema management therapies.

# Methods

## Volunteer demographics and ethical considerations

All subjects provided informed, written consent for this HIPAA and IRB-approved study. Healthy controls (N=8; age range=32-67 yrs) and patients with BCRL (**Table 1**; N=7; age range=52-76 yrs) were scanned at 3T (Philips, Best, The Netherlands) using dual-channel radiofrequency (RF) transmit and 16-channel torso coil (Torso XL) receive. Cancer treatment-related implants including breast implants, ports, and tissue expanders were screened by a board-certified radiologist when appropriate to ensure MRI safety.

Inclusion criteria for patients was BCRL (Stage 0-2) and lymph node resection. Only patients in Stage 0-2 were included as the motivation is to identify subtle microstructural changes that may precede clinical signs of lymphedema and disease progression. Additional patient information including circumferential arm measurements, medication regimen, duration since surgery, presence and duration of radiation therapy, number of lymph nodes removed during resection, breast reconstruction surgery, and handedness were all recorded. All patient information was obtained and interpreted by a certified lymphedema physical therapist.

## Experiment

In CEST MRI, information regarding protein concentration can be inferred by saturating exchangeable protons on the peptide backbone (here, amide protons resonating at +3.5 ppm from the water resonance), which exchange with water and attenuate the detectable water signal. CEST scanning was performed with a 3D gradient echo with multi-shot echo planar imaging (factor = 7), TR/TE = 166/6.6 ms, slices = 20, spatial resolution = $3 \times 3 \times 10$ mm$^3$ (anterior-posterior, right-left, foot-head). CEST preparation was performed by applying a single, Gaussian windowed sinc saturation pulse with peak $B_1$ = 1 μT and duration=75 ms at offset frequencies, $\Delta\omega = -6 - +6$ ppm with 0.25 ppm spacing with an additional 5 images obtained at ±80 ppm for CEST z-spectra normalization, similar to a previous clinical protocol optimized for brain tissue (18).

Structural scans were used to guide the placement of CEST imaging volume (**Fig. 1**), which spanned approximately 20 cm in the craniocaudal direction. A Diffusion-Weighted Imaging with Background Suppression (DWIBS) scan was utilized with scan parameters: spatial resolution=3×3×5 mm; *b*-value=800 s/mm$^2$; TR/TE/TI=8037/49.8/260 ms. The DWIBS scan suppresses static tissue signal by nulling the longitudinal component of the tissue magnetization following inversion recovery and enhances lymph node contrast by exploiting diffusion weighting, which sensitizes the contrast to tissue of different cellular density (19). The resulting image provides high contrast between lymph nodes and surrounding tissue. $T_2$*-weighted modified DIXON scanning was applied for structural tissue characterization and localization with scan parameters: 3D gradient echo, TR=3.4 ms, spatial resolution=1.0×1.3×3.0 mm. A $B_1$ map was obtained ($T_1$-weighted turbo gradient echo) with TR1/TR2=30/100 ms and identical spatial coverage and field of view as the CEST scans. In a subgroup of volunteers, high spatial resolution $T_2$-weighted (spectral adiabatic inversion recovery fat suppression, turbo spin echo; TR=3500 ms; TE=60 ms; spatial resolution = 0.4×0.5×5 mm) MRI was acquired.

## Imaging analysis

For CEST analysis, each RF offset of the CEST spectra was corrected for motion using a 3D six degree-of-freedom rigid body transformation. Post-processing proceeded using previously published routines (18). Briefly, for each voxel signal, $S(\Delta\omega)$, was normalized to the average signal obtained at ± 80 ppm ($S_0$) to generate a CEST z-spectrum. Next, to correct for $B_0$ inhomogeneity, a single Lorentzian lineshape (20) was fit to the CEST z-spectrum; the frequency offset corresponding to the Lorentzian minimum ($\Delta\omega_0$) was found and the z-spectrum was shifted such that $\Delta\omega_0 = 0$ ppm, analogous to the Water Saturation Shift Referencing (WASSR) approach (21). From the shifted z-spectrum, two indices were calculated. First, the standard APT asymmetry ($APT_A$) was determined as the difference between the normalized signals obtained at negative and positive offset frequencies, $S(-\Delta\omega)/S_0$ and $S(+\Delta\omega)/S_0$, respectively:

$$APT_A = \frac{S(-\Delta\omega) - S(+\Delta\omega)}{S_0} \quad [1]$$

Secondly, the difference between the Lorentzian fit and the data for all voxels was calculated, which was designated $APT_L$:

$$APT_L = \frac{L(-\Delta\omega) - S(+\Delta\omega)}{S_0} \quad [2]$$

where *L* denotes the Lorentzian fit to the data. For both the $APT_A$ and $APT_L$, the focus was on the values obtained between +3.75 − +3.25 ppm and −3.25 − −3.75 ppm, which reflect primarily the CEST effect between amide and water protons. The advantage of the $APT_L$ is that it is less sensitive to asymmetric contributions on the opposite (−ppm) side of the z-spectrum which could arise from lipid or exchange-mediated nuclear overhauser effects and magnetization transfer effects (22-25) which may confound APT asymmetry. Both $APT_A$ and $APT_L$ parameters were compared in this study. Finally, $B_1$ was calculated (26) from the $B_1$ maps in medial right and left arm regions (**Fig. 1**).

## Statistics

The primary statistical objective of this study was to assess the size of the APT effect in the affected and contralateral arms of BCRL patients and to contrast these values with asymmetry values observed in the right and left arms of age-matched control volunteers. A secondary aim was to assess whether variability in APT effect size could be explained by the extent of lymphatic compromise as quantified by clinical lymphedema stage. Descriptive statistics, including means, standard deviations, and ranges for continuous parameters, as well as percent and frequency for categorical parameters, were evaluated. Investigations for

Author Manuscript Author Manuscript Author Manuscript Author Manuscript

outliers and assumptions for statistical analysis, e.g., normality and homoscedasticity were also made. To test the primary statistical objective, a t-test and non-parametric Kruskal-Wallis test was applied between (i) the Lorentzian asymmetry values in patients and controls, (ii) APT effect sizes in the right versus left arms of controls or the affected versus contralateral arms of patients, and (iii) measured $B_1$ in right and left arms. Further, to understand asymmetry between limbs, Pearson's moment coefficient of skewness was calculated, which provides a measure of the asymmetry of the probability distribution of the APT effect size about its mean. As the sample size was modest, Cohen's d (standardized difference between means) was also calculated. Cohen's d was calculated separately for the $APT_L$ values for all lymphedematous arms and non-lymphedematous arms, as well for the ratio of the right/left $APT_L$ value in patients versus ratio of the lymphedematous/contralateral $APT_L$ in patients. To test the secondary objective, the APT effect size was compared with the lymphedema stage of patients. $P < 0.05$ was defined as significant for t-tests and Kruskal-Wallis tests. For Cohen's d, small, medium, and large effect sizes were delineated using the convention Cohen's d = 0.2, 0.5, and 0.8, respectively.

### Study approval

All subjects provided informed, written consent in accordance with the Vanderbilt University Institutional Review Board (IRB #111116).

## Results

**Fig. 1** shows the approximate location of the APT CEST slice placement relative to both a $T_2$-weighted structural scan (**Fig. 1A**), representative field map data (**Fig. 1B**), and the location of the axillary lymph nodes as demarcated on the DWIBS scan (**Fig. 1C**). High-spatial resolution imaging of axillary lymph nodes is included in **Fig. 1D**. The spatial coverage of the CEST scans (approximately identical to that of the $T_2$-weighted structural scan in **Fig. 1A**) is centered on the axillary lymph nodes and spans 100 mm in the craniocaudal direction. As there was a concern that $B_1$ would vary over this range, $B_1$ maps were obtained and highlight consistency in $B_1$ between medial portions of right and left arms, which are the regions of known interstitial protein accumulation and the regions of interest for this study. If $B_1$ was found to vary by more than two standard deviations from the ROI mean in any control, these regions were excluded from analyses. No mean $B_1$ difference between right and left arms of volunteers ($P = 0.48$); right/left $B_1$ (mean ± std) = $1.03 \pm 0.14$ was found. $B_1$ was found to be most symmetric between arms when the arms were placed on the chest rather than at the patients' sides. Position was controlled by supporting the proximal upper arms with a towel roll and Velcro™ straps around the torso coil. In **Fig. 1B**, the region-of-interest (ROI) is also shown (white; bottom right panel). The ROI includes both medial arms, and care was taken to avoid surrounding bones of the arm, shoulder, and chest wall. Tissue of the medial upper arm regions was not removed by resection in patients.

**Fig. 2** outlines the mechanism of the APT CEST effect (**Fig. 2A**) and also shows the $B_0$-corrected mean z-spectrum data (square markers) for the right (**Fig. 2B**) and left (**Fig. 2C**) arms of the control volunteers, along with the Lorentzian fit (solid line). Note the relative

Author Manuscript Author Manuscript Author Manuscript Author Manuscript

symmetry in APT effects between right and left arms, however the height of the z-spectrum does vary slightly, which is consistent with small differences in $B_1$ between the right and left arm. For this reason, we applied a Lorentzian fitting approach that accounts for voxel-wise differences in $B_1$. The relationship between the typical asymmetry approach (e.g., comparing the +ppm and –ppm APT data) and the Lorentzian approach (e.g., comparing the +3.75 − +3.25 ppm data to the Lorentzian fit at the −3.75 − −3.25 ppm data) are shown in **Fig. 2D** for each subject (right and left side data plotted as separate points). These two measurements correlate significantly on average (N=16; R=0.63; P=0.005), however there is approximately a two-fold increase in the variability of the $APT_A$ measures relative to $APT_L$, which was attributed to variations on the –ppm of the z-spectrum, consistent with asymmetric magnetization transfer (MT), nuclear overhauser effects, and/or noise. **Fig. 2E** shows representative $APT_L$ maps for the central slices of a control volunteer, displaying the typical range in $APT_L$ between healthy right and left arms.

**Fig. 3** shows the magnitude of the APT effect in right and left arms of control subjects (**Fig. 3A**) and individual subject line plots (**Fig. 3B**). In **Fig. 3C and Fig. 3D**, the same analysis is shown for the affected and contralateral arms of BCRL patients. A summary of clinical information on the patients is presented in **Table 2**. Both a two-tailed t-test and Kruskal-Wallis test revealed no significant difference between $APT_L$ or $APT_A$ in the right and left arms of healthy controls (P>0.05), but an increase in $APT_L$ (T-test P=0.033; Kruskwal-Wallis P=0.025) in the affected arms of patients. **Fig. 3E** shows the $APT_L$ asymmetry (e.g., difference between $APT_L$ in affected and contralateral arms of patients or right and left arms of controls). As can be seen, a strong trend on average is found in the patients relative to the controls, however patient data also have added variability. The skewness (third central moment of asymmetry values, **Fig. 3E**, divided by the cube of the standard deviation) was elevated for patients (0.88) relative to controls (0.34). Cohen's d revealed a large effect size when considering both the magnitude of the $APT_L$ value in lymphedematous arms to $APT_L$ in all other other arms (Cohen's d = 2.4) and also between the ratio of lymphedematous/ contralateral $APT_L$ and ratio of right/left $APT_L$ in controls volunteers (Cohen's d = 1.1). To better understand variability in patient contrast, we considered potential contributing clinical factors.

**Fig. 4A** shows $APT_L$ maps from two central slices for Patient 1 (**Table 2**). Patient 1 is a right hand dominant 42 yo/F with stage 0 (subclinical) lymphedema on the left and stage 2 lymphedema on the right. Her pertinent history includes chemotherapy and left sided mastectomy, axillary dissection removing 12 lymph nodes and reconstructive surgery following left sided breast cancer 11 years prior to participating in this study, followed by a right simple mastectomy with one sentinel lymph node biopsy due to right sided breast cancer 3.5 years prior to the CEST scan. She is currently taking Tamoxifen for hormone therapy. $APT_L$ asymmetry between the medial portion of the lymphedematous arm and contralateral arm is observed, which manifests as a larger signal attenuation in the +3.75 − +3.25 ppm range on the z-spectrum.

**Fig. 4B** shows $APT_L$ maps for Patient 3 (**Table 2**). Patient 3 is a right hand dominant 76 yo/F with right-sided stage 1 lymphedema who underwent right total mastectomy and axillary lymphadenectomy (resecting 16 axillary lymph nodes) followed by chemotherapy

Author Manuscript Author Manuscript Author Manuscript Author Manuscript

and radiation 7.5 years prior to participating in this study. She is currently taking Arimidex. Similar to Patient 1, $APT_L$ asymmetry between the internal portion of the lymphedematous arm and contralateral arm is observed.

**Fig. 4C** shows $APT_L$ maps for Patient 4. Patient 4 is a right hand dominant 46 yo/F with subclinical lymphedema six months after undergoing chemotherapy and a right total mastectomy with reconstruction, sentinel lymph node biopsy followed by axillary lymphadenectomy resecting a total of 24 axillary lymph nodes. Similar to Patients 1 and 3, this patient also demonstrates asymmetric $APT_L$ between limbs relative to controls, but did not meet clinical criteria (**Table 1**) for stage 1 lymphedema. However, the large number of 24 nodes removed placed this patient at high risk of BCRL, and evidence of protein accumulation is seen in the $APT_L$ images. At one-year follow-up this patient progressed to Stage 1 lymphedema.

Finally, **Fig. 5** shows the relationship between the APT effect size and the category of volunteer (healthy controls, and Stage 0-2 BCRL patients). In this analysis, patient arms with lymph nodes removed but who did not meet clinical criteria for BCRL (**Table 1**) were categorized as Stage 0. A trend for increasing APT effect size with more advanced impairment is observed. Formal statistical tests were not performed on these data owing to the relatively small sample size per group; therefore, these data support, but do not confirm, that APT contrast may increase with increasing BCRL stage.

## Discussion

In terms of medical research, the lymphatic system is one of the most neglected bodily systems relative to its role in disease, which has resulted in an incomplete understanding of lymphatic functioning in health and disease. The purpose of this study was to evaluate for the first time whether noninvasive CEST MRI, which has demonstrated clinical potential in brain (27,28), liver (29), head/neck (30), and breast applications (31), can be translated to the human lymphatic system to identify known lymphatic dysfunction following breast cancer treatment. Relative to healthy controls, increased APT asymmetry between healthy and lymphedematous arms was observed in patients with BCRL, and furthermore a trend for a relationship between $APT_L$ effect size and lymphedema stage was found. These data provide justification for further investigation of APT CEST in BCRL patients including the at-risk population and other patients where there is potential for lymphatic compromise. The long-term goal of this work is to demonstrate abilities to accurately record structural and functional observables of lymphatic dysfunction, derived from noninvasive MRI equipment available at most hospitals, which can serve as trial end points for randomized clinical trials of lymphedema prevention and management therapies.

### Overview of lymphatic vessel anatomy

The lymphatic system plays a crucial role for maintaining fluid balance, nutritional function, and host defense. It is useful to understand the most salient aspects of the lymphatic vasculature prior to considering the relevance of existing MRI approaches for assessing lymphatic function. A detailed review of lymphatic functionality can be found in the literature (2). Briefly, lymphatic vessels, or lymphatics, can be differentiated into *lymph*

Author Manuscript Author Manuscript Author Manuscript Author Manuscript

*capillaries*, *precollectors*, *collectors*, and *trunks*. *Lymph capillaries* originate near blood capillaries in the interstitium and absorb macromolecules through open junctions in lymph capillary endothelial cells. Open junctions permit fluid entrance into the lymph capillaries when the interstitial pressure changes due to elevations in blood capillary filtrate. Capillary filtrate constitutes protein rich fluid that enters the interstitium from the arterial capillaries. Semi-elastic fibers, or anchoring filaments, which connect the lymph capillaries to the surrounding connective tissue, respond to changes in interstitial pressure causing junctions of lymph capillaries to open and the protein-rich capillary filtrate to enter the lymphatic capillaries from the interstitium. *Lymph precollectors* join the lymph capillaries and *lymph collectors*, or larger lymphatic vessels (0.1-0.6 mm in diameter), and function to transport lymph fluid from the lymphatic capillaries to the lymph collectors. Lymph collectors subsequently transport lymphatic fluid to the lymph nodes and lymphatic trunks. The lymph collectors contain valves that ensure the unidirectional flow of fluid, as well as lymphangions which contract (autonomic contraction; 10-12 contractions per minute) to assist with lymph flow. The lymphatic collectors forward lymph fluid to the *lymphatic trunks* and *lymph nodes*. Humans have on average 600-700 lymph nodes, with the majority located in head and neck (cervical and supraclavicular), intestinal (inguinal) and armpit (axilla) regions. Afferent lymph collectors transport lymphatic fluid to the nodes, where it is filtered, whereas efferent lymph collectors transport fluid from the node either to lymphatic trunks or additional nodes. Lymphatic fluid is ultimately returned to the blood circulation through the venous system. Approximately 75% of lymphatic fluid is returned via the thoracic duct into the left venous angle (left internal jugular and left subclavian vein), whereas approximately 25% of lymphatic fluid is returned via the right lymphatic duct into the right venous angle (right internal jugular and subclavian veins).

## Relevance of lymphatic functioning to disease

Disruption to the above lymphatic flow processes are central to a variety of diseases. Inefficient or impaired lymph drainage can result from chronic cardiovascular disease and may persist even following successful therapy for cardiovascular symptoms depending on the extent of damage. Additionally, the importance of lipid absorption in intestinal lymphatics has been well-documented (32), and lipid absorption may be relevant to non-intestinal lymphatics (33), and as such lymphatic dysfunction may contribute in different ways to obesity and successful obesity treatment. It is well-known that lymphatics are the primary route for the spread of metastatic cancer, and a better understanding of the manner in which cancer cells enter the lymphatics could be crucial from improving clinical outcomes in cancer patients. The lymphatics play a key role in immune response and antigen transport, and similarly with the progression of autoimmune disorders. Correspondingly, the lymphatic system is fundamental to some of the most debilitating conditions of society today (e.g., cardiovascular disease, cancer spread, obesity and autoimmune dysfunction) yet imaging tools to characterize lymphatic structure and function substantially lag in development relative to those applied to other bodily processes and diseases.

In terms of secondary lymphedema as evaluated in this study, mechanical insufficiency is caused by a larger lymphatic load relative to lymphatic capacity. In patients with BCRL, this is due to a reduction in lymphatic capacity following lymph node removal, radiation therapy,

Author Manuscript Author Manuscript Author Manuscript Author Manuscript

and damage to the lymphatics. This mechanical insufficiency leads to protein accumulation in the interstitial space and corresponding limb swelling of protein-rich fluid. It has not been possible to measure this protein accumulation using noninvasive imaging to date. Here, we have provided evidence that CEST MRI (13,17) can be used to visualize this protein-weighted water signal in different stages of lymphedema progression. Furthermore, we have observed changes in CEST contrast in the affected arms of BCRL patients (Stage 0-2) relative to the contralateral arm and compared to healthy controls, even in the absence of irreversible changes in lymph structure or limb swelling (Stage 0). These findings suggest that CEST contrast may provide a biomarker of lymphatic dysfunction even in early stages of disease.

### Relevance of noninvasive lymphatic imaging

The clinical relevance of this possibility is that in health, the lymphatic transport capacity (i.e., highest possible lymphatic flow per unit time) exceeds the lymphatic load by as much as a factor of ten (34) providing the body with a reserve capacity in the event of temporarily increased lymphatic loads, such as during infection. Given this reserve, the lymphatic system may effectively compensate for a small increase in lymphatic load or reduction in lymphatic transport capacity, as is the case following lymph node removal or damage. Once the lymphatic system is no longer able to fully compensate for the lymphatic load generated, protein-rich fluid will start to accumulate in the interstitium and eventually swelling will become evident. Therefore, an ability to measure small changes in interstitial protein accumulation, or changes in lymphatic flow velocity, could be beneficial for early detection of lymphatic dysfunction, thereby providing clinicians with evidence of lymphatic impairment before clinical signs of swelling develop. Decongestive therapeutic approaches in the early stage (Stage 0) may be useful for addressing early lymphatic dysfunction and offsetting the progression to observable signs of lymphedema (Stage 1-3) in this at-risk population. Using these noninvasive biomarkers of lymphatic function and dysfunction may help to more comprehensively evaluate the impact therapies have on the lymphatic system, thereby influencing the standard of care for lymphedema prevention and management.

In addition to the CEST approach outlined in this study, it has been shown that spin labeling may also be useful for non-invasively assessing lymphatic flow velocity (35). For perfusion quantification, a spin labeling postlabeling delay of only 1.5-2s is generally required owing to the relatively fast inflow of blood water through the arterial system; the spin labeling difference magnetization owing to perfusion is small at only 1–2% of unlabeled tissue signal. This signal arises from the small amount of perfusion-weighted contrast relative to total signal intensity and the decay of the magnetic label with blood water longitudinal relaxation time ($T_1$~1.7s for arterial blood water at 3.0T). Importantly, a longer $T_1$ is required to image flow from fluids with lower velocity, such as lymphatic fluid where the flow velocity is several factors slower than that of blood. The $T_1$ of lymphatic fluid is more than twice as long as that of blood water at 3.0T ($T_1$=3100±160 ms) (35), and furthermore that this longer $T_1$ enables longer postlabeling delay times, thereby allowing for visualization of lymphatic fluid flow of less than 1 cm/min. Motivation for this technique has been demonstrated and consistent changes in lymphatic flow properties are detectable *in vivo* under (i) conditions of cuff-induced lymph flow manipulation, and (ii) in affected vs.

Author Manuscript Author Manuscript Author Manuscript Author Manuscript

unaffected arms of BCRL patients (35). Ongoing work could also exploit principles of lymphatic inflow (analogous to time-of-flight magnetic resonance angiography) to assess lymphatic flow velocity into lymph nodes over an even larger temporal scale.

The overreaching hypothesis of this line of research is that similar to other diseases such as stroke, Alzheimer's disease, and cancer, subtle preclinical changes in system function precede observable structural changes and symptoms in BCRL, and other conditions where lymphatic compromise is implicated. Accurate measurement of these early changes is fundamental to identifying patients at highest risk of lymphedema and guiding preventative therapy. Furthermore the sensitivity of these measures should allow us to more precisely understand therapy impact on lymphatic processing. To test this possibility, it will be necessary to grow imaging technologies that are capable of noninvasively understanding mechanisms of lymphedema onset and therapy response. These methods may hold significance in two important ways. Firstly, they will demonstrate the utility of using noninvasive MRI for detecting changes in lymphatic structure *and* function. As these methods require imaging equipment available at most hospitals, methods can be disseminated to allow for large-scale trials of optimized lymphedema therapy and prevention in the future. Secondly, this work can be used to evaluate the impact that common lymphedema therapies, e.g., manual lymphatic drainage (MLD) and compression devices and modalities (2), have on lymphatic system structure and function, as well as the direct impact on lymphatic function when such therapies are implemented early to address early signs of lymphedema, i.e. the application of a day-time compression sleeve or self-MLD as a response to early signs of lymphedema.

## Technical considerations

This study represents the first application of CEST in patients with BCRL and several technical considerations should be considered when interpreting the study findings.

Our hypothesis was that increased APT effects should be observed in lymphedematous arms owing to increased interstitial protein accumulation and an increase in the amount of exchangeable amide protons. However, over a physiological range it should also be noted that the exchange rate between amide and water protons is base catalyzed, and therefore differences in pH could also contribute. To our knowledge, there is no basis for a substantial pH change in the interstitium of lymphedematous vs. healthy limbs, however pH was not measured as part of this study and as such this possibility cannot be eliminated.

The findings of this study should be interpreted within the context of the total sample size. The purpose of our study was to determine whether APT CEST could be applied in extremity regions of lymphedema patients and also whether this approach provided unique contrast in patients relative to controls, and in a manner consistent with disease stage and symptomatology. The data provided support this conclusion, however larger studies are required to understand the utility of APT CEST as a prognostic tool or biomarker. Additionally, our sample size did not allow for a rigorous statistical evaluation of the relationship between APT contrast and BCRL stage, which should be the topic of future work with larger sample sizes.

Author Manuscript

Author Manuscript

Author Manuscript

Author Manuscript

We measured no significant difference in $B_1$ between right and left arms of controls, or lymphedematous and non-lymphedematous limbs of patients on average and therefore it is unlikely that the lateralizing trend observed in patients is due solely to $B_1$. A Gaussian-windowed sinc saturation pulse with peak $B_1$ = 1 μT and duration=75 ms with a dual RF transmit body coil was utilized here; regional variability in $B_1$ will likely reduce the $B_1$ in some regions and both narrow the CEST z-spectrum and reduce the APT effect. To reduce this confound, we focused on medial arm regions where $B_1$ was highest and most homogeneous (**Fig. 1**), and also where interstitial protein accumulation is expected. Future work may benefit by increasing $B_1$ to ensure acceptable saturation (e.g., $B_1$ > 1 μT) even in the presence of heterogenous pulse profiles, correcting for $B_1$ in post-processing (36), and utilizing more complex RF shimming algorithms for the CEST pre-saturation pulse. Additional improvements could be made by using parallel transmit (37) and tailored RF pulses (38) to improve $B_1$ and flip angle uniformity in the arms. RF shim weights and tailored pulses could be designed by including only the arms and axilla in the pulse optimization.

Finally, the large FOV required (right/left = 500-600 mm) for imaging bilateral arms and axilla is beyond the default “shutter” window of the Philips scanner, used here. This shutter window can be extended as a reconstruction control parameter. It should be ensured that the shutter window is sufficiently large to enable imaging of both arms, as otherwise lateral arm signal may be removed, especially in larger patients.

## Conclusion

Impairment of the lymphatics is known to reduce quality of life in some of the most crippling diseases of the 21st century. Despite this, lymphatic functioning is not nearly as well understood as the majority of other bodily systems, partly owing to a lack of sensitive imaging technologies that can be applied using standard clinical equipment. In this work, we translated structural and functional (APT CEST) MRI methods to understand whether lymphatic compromise could be visualized using emerging functional imaging methods that have shown clinical relevance in brain, breast, and liver disease. We provide evidence supporting the ability of APT CEST to provide contrast consistent with lateralizing disease in patients with breast cancer treatment-related lymphedema, thereby motivating the further investigation of these and similar methods for clinical lymphedema trials.

## Acknowledgements

We thank William Grissom for helpful discussion regarding $B_1$ heterogeneity, as well as Kristen George-Durrett, Leslie McIntosh, Chuck Nockowski, David Pennell, and Clair Kurenbach for experimental support. Funding provided by: NIH/NINR: 1R01NR015079, NIH/NEI: 1R01EY023240, NIH/NINDS: 1R21NS087465, Vanderbilt Institute for Clinical Research (VICTR) VR8745.

**Funding:** NIH/NINR: 1R01NR015079, NIH/NEI: 1R01EY023240, NIH/NINDS: 1R21NS087465, Vanderbilt Institute for Clinical Research (VICTR) VR8745

## References

1. Mortimer PS, Rockson SG. New developments in clinical aspects of lymphatic disease. J Clin Invest. 2014; 124(3):915–921. [PubMed: 24590276]

Author Manuscript Author Manuscript Author Manuscript Author Manuscript

2. Zuther JE, Norton S, Armer JM. Lymphedema management : the comprehensive guide for practitioners. Stuttgart: Thieme. 2013

3. DiSipio T, Rye S, Newman B, Hayes S. Incidence of unilateral arm lymphoedema after breast cancer: a systematic review and meta-analysis. Lancet Oncol. 2013; 14(6):500–515. [PubMed: 23540561]

4. Moseley AL, Carati CJ, Piller NB. A systematic review of common conservative therapies for arm lymphoedema secondary to breast cancer treatment. Annals of oncology : official journal of the European Society for Medical Oncology / ESMO. 2007; 18(4):639–646. [PubMed: 17018707]

5. Carson CJ, Coverly K, Lasker-Hertz S. The incidence of co-morbidities in the treatment of lymphedema. J Oncol Manag. 1999; 8(4):13–17. [PubMed: 10539520]

6. Ridner SH. Breast cancer treatment-related lymphedema--A continuing problem. J Support Oncol. 2006; 4(8):389–390. [PubMed: 17004512]

7. Torres Lacomba M, Yuste Sanchez MJ, Zapico Goni A, Prieto Merino D, Mayoral del Moral O, Cerezo Tellez E, Minayo Mogollon E. Effectiveness of early physiotherapy to prevent lymphoedema after surgery for breast cancer: randomised, single blinded, clinical trial. Bmj. 2010; 340:b5396. [PubMed: 20068255]

8. Stout NL, Weiss R, Feldman JL, Stewart BR, Armer JM, Cormier JN, Shih YC. A systematic review of care delivery models and economic analyses in lymphedema: health policy impact (2004-2011). Lymphology. 2013; 46(1):27–41. [PubMed: 23930439]

9. Chen CM, Cano SJ, Klassen AF, King T, McCarthy C, Cordeiro PG, Morrow M, Pusic AL. Measuring quality of life in oncologic breast surgery: a systematic review of patient-reported outcome measures. The breast journal. 2010; 16(6):587–597. [PubMed: 21070435]

10. Liu N, Wang C, Sun M. Noncontrast three-dimensional magnetic resonance imaging vs lymphoscintigraphy in the evaluation of lymph circulation disorders: A comparative study. J Vasc Surg. 2005; 41(1):69–75. [PubMed: 15696047]

11. Rane S, Donahue PM, Towse T, Ridner S, Chappell M, Jordi J, Gore J, Donahue MJ. Clinical Feasibility of Noninvasive Visualization of Lymphatic Flow with Principles of Spin Labeling MR Imaging: Implications for Lymphedema Assessment. Radiology. 2013 [Epub ahead of print].

12. Kwee TC, Takahara T, Ochiai R, Nievelstein RA, Luijten PR. Diffusion-weighted whole-body imaging with background body signal suppression (DWIBS): features and potential applications in oncology. Eur Radiol. 2008; 18(9):1937–1952. [PubMed: 18446344]

13. Ward KM, Aletras AH, Balaban RS. A new class of contrast agents for MRI based on proton chemical exchange dependent saturation transfer (CEST). J Magn Reson. 2000; 143(1):79–87. [PubMed: 10698648]

14. Dula AN, Smith SA, Gore JC. Application of Chemical Exchange Saturation Transfer (CEST) MRI for Endogenous Contrast at 7 Tesla. J Neuroimaging. 2013 [Epub ahead of print].

15. van Zijl PC, Zhou J, Mori N, Payen JF, Wilson D, Mori S. Mechanism of magnetization transfer during on-resonance water saturation. A new approach to detect mobile proteins, peptides, and lipids. Magn Reson Med. 2003; 49(3):440–449. [PubMed: 12594746]

16. Zhou J, Wilson DA, Sun PZ, Klaus JA, Van Zijl PC. Quantitative description of proton exchange processes between water and endogenous and exogenous agents for WEX, CEST, and APT experiments. Magn Reson Med. 2004; 51(5):945–952. [PubMed: 15122676]

17. Meeske KA, Sullivan-Halley J, Smith AW, McTiernan A, Baumgartner KB, Harlan LC, Bernstein L. Risk factors for arm lymphedema following breast cancer diagnosis in Black women and White women. Breast Cancer Res Treat. 2009; 113(2):383–391. [PubMed: 18297429]

18. Tietze A, Blicher J, Mikkelsen IK, Ostergaard L, Strother MK, Smith SA, Donahue MJ. Assessment of ischemic penumbra in patients with hyperacute stroke using amide proton transfer (APT) chemical exchange saturation transfer (CEST) MRI. NMR Biomed. 2014; 27(2):163–174. [PubMed: 24288260]

19. Klomp DW, Dula AN, Arlinghaus LR, Italiaander M, Dortch RD, Zu Z, Williams JM, Gochberg DF, Luijten PR, Gore JC, Yankeelov TE, Smith SA. Amide proton transfer imaging of the human breast at 7T: development and reproducibility. NMR Biomed. 2013; 26(10):1271–1277. [PubMed: 23559550]

Author Manuscript

Author Manuscript

Author Manuscript

Author Manuscript

20. Mulkern RV, Williams ML. The general solution to the Bloch equation with constant rf and relaxation terms: application to saturation and slice selection. Med Phys. 1993; 20(1):5–13. [PubMed: 8455512]
21. Kim M, Gillen J, Landman BA, Zhou J, van Zijl PC. Water saturation shift referencing (WASSR) for chemical exchange saturation transfer (CEST) experiments. Magn Reson Med. 2009; 61(6): 1441–1450. [PubMed: 19358232]
22. Jones CK, Huang A, Xu J, Edden RA, Schar M, Hua J, Oskolkov N, Zaca D, Zhou J, McMahon MT, Pillai JJ, van Zijl PC. Nuclear Overhauser enhancement (NOE) imaging in the human brain at 7T. Neuroimage. 2013; 77:114–124. [PubMed: 23567889]
23. Hua J, Jones CK, Blakeley J, Smith SA, van Zijl PC, Zhou J. Quantitative description of the asymmetry in magnetization transfer effects around the water resonance in the human brain. Magn Reson Med. 2007; 58(4):786–793. [PubMed: 17899597]
24. Jin T, Kim SG. Advantages of chemical exchange-sensitive spin-lock (CESL) over chemical exchange saturation transfer (CEST) for hydroxyl- and amine-water proton exchange studies. NMR Biomed. 2014; 27(11):1313–1324. [PubMed: 25199631]
25. Desmond KL, Stanisz GJ. Understanding quantitative pulsed CEST in the presence of MT. Magn Reson Med. 2012; 67(4):979–990. [PubMed: 21858864]
26. Yarnykh VL. Actual flip-angle imaging in the pulsed steady state: a method for rapid three-dimensional mapping of the transmitted radiofrequency field. Magn Reson Med. 2007; 57(1):192–200. [PubMed: 17191242]
27. Flament J, Geffroy F, Medina C, Robic C, Mayer JF, Meriaux S, Valette J, Robert P, Port M, Le Bihan D, Lethimonnier F, Boumezbeur F. In vivo CEST MR imaging of U87 mice brain tumor angiogenesis using targeted LipoCEST contrast agent at 7 T. Magn Reson Med. 2013; 69(1):179–187. [PubMed: 22378016]
28. Sheth VR, Li Y, Chen LQ, Howison CM, Flask CA, Pagel MD. Measuring in vivo tumor pHe with CEST-FISP MRI. Magn Reson Med. 2012; 67(3):760–768. [PubMed: 22028287]
29. van Zijl PC, Jones CK, Ren J, Malloy CR, Sherry AD. MRI detection of glycogen in vivo by using chemical exchange saturation transfer imaging (glycoCEST). Proc Natl Acad Sci U S A. 2007; 104(11):4359–4364. [PubMed: 17360529]
30. Yuan J, Chen S, King AD, Zhou J, Bhatia KS, Zhang Q, Yeung DK, Wei J, Mok GS, Wang YX. Amide proton transfer-weighted imaging of the head and neck at 3 T: a feasibility study on healthy human subjects and patients with head and neck cancer. NMR Biomed. 2014; 27(10):1239–1247. [PubMed: 25137521]
31. Cai K, Xu HN, Singh A, Moon L, Haris M, Reddy R, Li LZ. Breast cancer redox heterogeneity detectable with chemical exchange saturation transfer (CEST) MRI. Mol Imaging Biol. 2014; 16(5):670–679. [PubMed: 24811957]
32. Holt S, Guram M, Smith M, Skinner HA. Computer assessment of life-style in a gastroenterology clinic. Dig Dis Sci. 1992; 37(7):993–996. [PubMed: 1618069]
33. Brorson H, Ohlin K, Olsson G, Nilsson M. Adipose tissue dominates chronic arm lymphedema following breast cancer: an analysis using volume rendered CT images. Lymphat Res Biol. 2006; 4(4):199–210. [PubMed: 17394403]
34. Olszewski, W. Peripheral lymph : formation and immune function. CRC Press; Boca Raton, Fla.: 1985. p. 167
35. Rane S, Donahue P, Jordi J, Gore JC, Donahue MJ. Noninvasive Characterization of Lymphatic Flow Velocity Using Principles of Spin Labeling. International Society for Magnetic Resonance in Medicine. 2012:575.
36. Singh A, Cai K, Haris M, Hariharan H, Reddy R. On B1 inhomogeneity correction of in vivo human brain glutamate chemical exchange saturation transfer contrast at 7T. Magn Reson Med. 2013; 69(3):818–824. [PubMed: 22511396]
37. Katscher U, Bornert P, Leussler C, van den Brink JS. Transmit SENSE. Magn Reson Med. 2003; 49(1):144–150. [PubMed: 12509830]
38. Grissom WA, Khalighi MM, Sacolick LI, Rutt BK, Vogel MW. Small-tip-angle spokes pulse design using interleaved greedy and local optimization methods. Magn Reson Med. 2012; 68(5): 1553–1562. [PubMed: 22392822]

Author Manuscript Author Manuscript Author Manuscript Author Manuscript

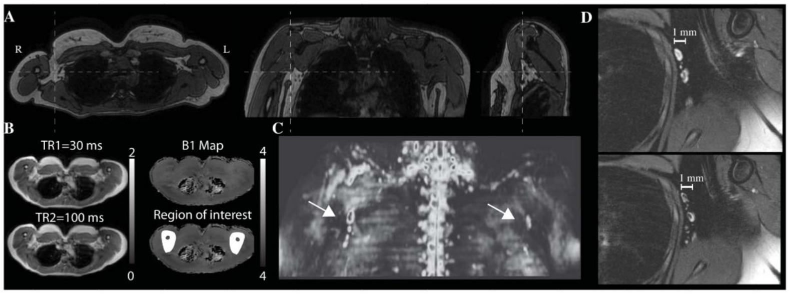

**Figure 1. Spatial coverage and planning of lymphatic imaging**

(A) Orthogonal representations of 3D T2-weighted mDIXON scans, which are used for identifying the approximate location of axillary lymph nodes and surrounding muscle and fat structure. (B) Multi-TR B1 maps for one control subjectshowing typical B1 consistency between right and left arms. In the bottom right panel, an example region-of-interest (ROI) used for amide proton transfer (APT) analysis is shown (white). (C) The 3D Diffusion Weighted Imaging with Background Suppression (DWIBS) scan (maximum intensity projection) demarcates the approximate location of axillary lymph nodes, and (E) the high spatial resolution fat-suppressed T2-weighted scans highlights structural characteristics of the lymph nodes. These images can be acquired non-invasively using standard MRI hardware in less than 10 min, and can be used for guiding assessment of functional changes in human lymphatics.

Author Manuscript

Author Manuscript

Author Manuscript

Author Manuscript

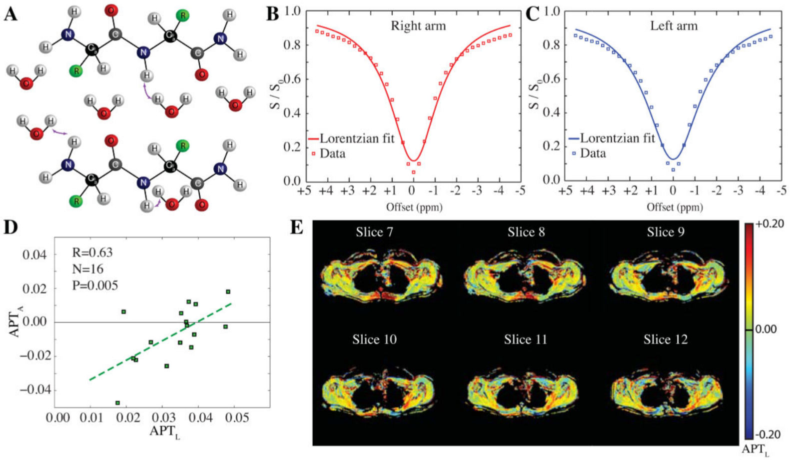

**Figure 2. Amide proton transfer (APT) effects in healthy control volunteers**

(A) Amide protons ([NH]~100 mM) which resonate at +3.5 ppm from the water resonance are in constant exchange (rate~40 Hz) with surrounding bulk water ([$H_2O$]~110M). By selectively irradiating at the amide resonance prior to water detection, NH proton magnetization is reduced, which attenuates the detectable water signal following exchange. This effect is commonly visualized in the CEST z-spectrum (B,C), in which water signal following different radiofrequency (RF) pre-pulse offsets is shown. The lineshape is influenced by broad nuclear overhauser (NOE), T1/T2, and RF spillover effects, with small, additional attenuation apparent at +3.5 ppm owing to proton exchange. Mean (N=8) control z-spectra for (B) right and (C) left arms, along with Lorentzian fits. The squares denote acquired data whereas the solid lines denote the Lorentzian fit. The Lorentzian fit reflects information of $B_1$, $T_1$, and $T_2$, however not exchange and therefore provides a reference for exchange effects. (D) Both the Lorentzian APT analysis ($APT_L$) and Asymmetry APT analysis ($APT_A$) provide similar information ($P<0.05$) in control volunteers, however the variation in the $APT_L$ approach is much smaller owing to a reduction of sensitivity to NOE and magnetization transfer effects on the –ppm side of the z-spectrum. Right and left arms are plotted as separate data points (16 data points total). (E) $APT_L$ maps from a representative control volunteer (central slices covering axilla shown), which demonstrate the range of consistency between $APT_L$ measures in right and left axilla.

Author Manuscript
Author Manuscript
Author Manuscript
Author Manuscript

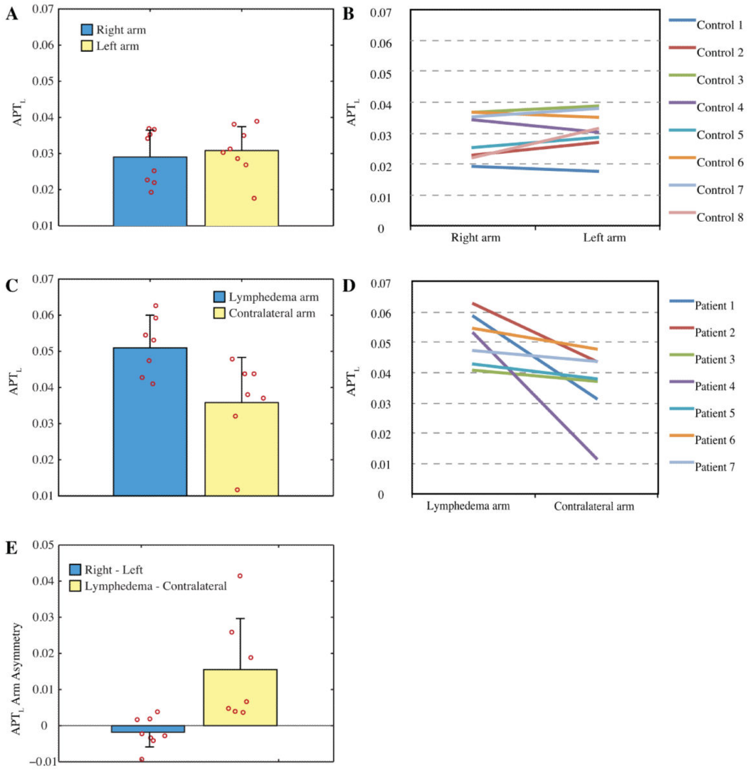

**Figure 3. Amide proton transfer effects in healthy and lymphedematous arms**

(A-B) The size of the APT effect is similar in right and left arms of healthy control subjects, but (C-D) increased in lymphedematous arms, on average, of patients with BCRL ($P<0.05$). Note the range of APT contrast in patients (red circles; Fig. C), however the consistent asymmetry observed between the lymphedematous arm and contralateral arm (D). (E) The per-subject asymmetry of the APT$_L$ effect is near zero in control volunteers, but significantly ($P<0.05$) elevated in BCRL patients. Red circles denote individual subject data and bars denote one standard deviation.

Author Manuscript Author Manuscript Author Manuscript Author Manuscript

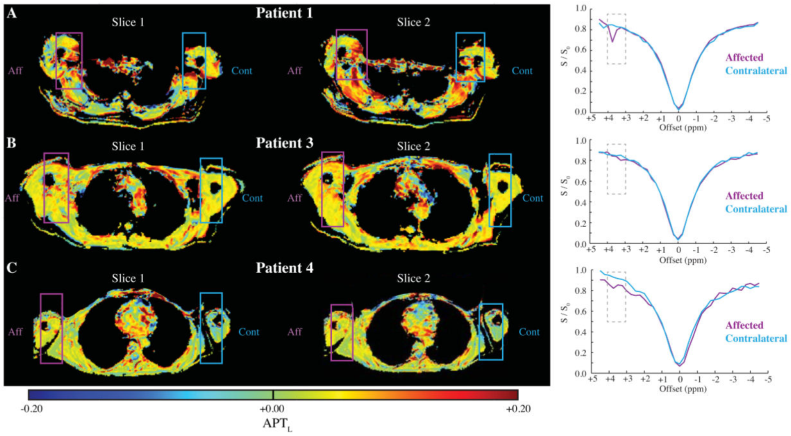

**Figure 4. Amide proton transfer (APT) effects in patients**

APT effect size is observed to be elevated in lymphedemetaous arms relative to contralateral arms, most notably subdermally on the medial aspect of upper arm. Breast tissue has been masked out owing to differential contrast from reconstructive surgery. Corresponding z-spectra are shown to the right, which denote a reduction in signal intensity in the region of the APT effect (+3.75 to +3.25 ppm range). Patient information is discussed in detail in the text and also in **Table 2**.

Author Manuscript Author Manuscript Author Manuscript Author Manuscript

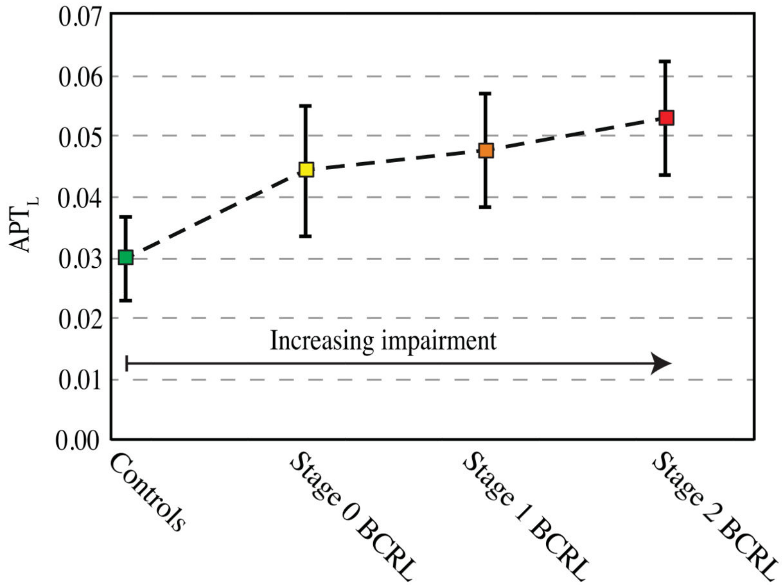

**Figure 5. Relationship between amide proton transfer (APT) effect size and clinical measures of impairment as defined by breast cancer treatment-related lymphedema (BCRL) stage (Table 1)**

Data are taken from all controls in the control group (green), and limbs of patients with node removal (e.g., both arms from patient 1 and 6 are included owing to bilateral node resection). Data suggest that APT contrast increases with increasing lymphatic impairment, and differences between control arms and Stage 0 BCRL patients are suggested. Additional data in a larger volume of patients, also controlling for duration since node resection and other risk factors (e.g., radiation therapy, age, sarcoma, cellulitis and obesity) are likely necessary to fully understand the relationship between APT contrast and lymphatic compromise. Bars denote one standard deviation.

Author Manuscript

Author Manuscript

Author Manuscript

Author Manuscript

## Table 1

Criteria for breast cancer treatment-related lymphedema (BCRL) staging.

| | **Defining clinical characteristics of BCRL in patients undergoing axillary lymph node dissection with/without radiation therapy** |
|---|---|
| Stage 0 | No observable lymphedema as defined by less than 2 cm difference in arm circumference between the involved and uninvolved arms. |
| Stage 1 | Reversible lymphedema defined as greater than 2 cm difference in arm circumference between the involved and uninvolved arms. Other criteria: Fibrosis: none or minimal; Pitting: pits on pressure; Elevation: reduces edema; Skin: no change |
| Stage 2 | Stage I criteria with Fibrosis: moderate; Pitting: may be present; Elevation: does not fully reduce edema (minimal to no reduction); Skin: no change |
| Stage 3 | The tissue is hard (fibrotic) and pitting is absent. Skin changes such as thickening, hyperpigmentation, increased skin folds, fat deposits and warty overgrowths develop |

Author Manuscript Author Manuscript Author Manuscript Author Manuscript

## Table 2

Clinical demographics of patients.

| **Study ID** | **Sex** | **Age at Scan (yrs)** | **Lymphedema Side** | **Lymphedema stage** | **Number nodes removed (left)** | **Number nodes removed (right)** | **Hand Dominance** | **Noted comorbidities** | **History of Chemotherapy** | **History of Radiation** | **Pertinent Medications** | **Time from Node Removal to Scan Date (years & months)** | **Lymphedema Management Stage** |
|---|---|---|---|---|---|---|---|---|---|---|---|---|---|
| Patient 1 | F | 42 | Right | 2 | 12 | 1 | Right | Bilatcral lymphedema risk | Yes | No | Tamoxifen | Left: 10years& 9months<br>Right: 3years and 6months | Self management stage, at time of scan recommended PT for additional CDT |
| Patient 2 | F | 60 | Right | 2 | 0 | 23 | Right | Metastatic recurrence in R axillary fibroadipose tissue, pleural effusion, ascites | Yes | No | Denosumab (Xgeva) | 2 years & 6months | Self management stage |
| Patient 3 | F | 76 | Right | 1 | 0 | 16 | Right | None noted | Yes | Yes | Arimidex | 7 years & 7months | Self management stage |
| Patient 4 | F | 46 | Right | 0 | 0 | 24 | Right | None noted | Yes | No | Tamoxifen | 6 months | Self management stage |
| Patient 5 | F | 58 | Right | 2 | 0 | 14 | Right | None noted | Yes | Yes | | 1 year & 4 months | Self management stage |
| Patient 6 | F | 55 | Left | 1 | 7 | 1 | Right | Bilateral lymphedema risk | Yes | No | | Left: 4years & 3months<br>Sight: 3 years & 8 months | Self management stage |
| Patient 7 | F | 60 | Left | 2 | 0 | 18 | Right | cellulitis - multiple bouts of cellulitis when first developed lymphedcma, no further cellulitis since receiving lymphodoma therapy | Yes | No | | 12 years | Self management stage, reecives MLD from trained massage therapist monthly |